JACS
JOURNAL OF THE AMERICAN CHEMICAL SOCIETY

Article

pubs.acs.org/JACS

Visualizing Compartmentalized Cellular Mg^{2+} on Demand with Small-Molecule Fluorescent Sensors

Jessica J. Gruskos,[†] Guangqian Zhang,[†] and Daniela Buccella*

Department of Chemistry, New York University, New York, New York 10003, United States

Supporting Information

ABSTRACT: The study of intracellular metal ion compartmentalization and trafficking involved in cellular processes demands sensors with controllable localization for the measurement of organelle-specific levels of cations with subcellular resolution. We introduce herein a new two-step strategy for in situ anchoring and activation of a fluorescent Mg^{2+} sensor within an organelle of choice, using a fast fluorogenic reaction between a tetrazine-functionalized pro-sensor, Mag-*S*-Tz, and a strained bicyclononyne conjugated to a genetically encoded HaloTag fusion protein of known cellular localization. Protein conjugation does not affect the metal-binding properties of the *o*-aminophenol-*N*,*N*,*O*-triacetic acid (APTRA)-based fluorescent indicator, which displays a dissociation constant K_d = 3.1 mM suitable for the detection of low millimolar concentrations of chelatable Mg^{2+} typical of the intracellular environment. We demonstrate the application of our sensing system for the ratiometric detection of Mg^{2+} in target organelles in HEK 293T cells, providing the first direct comparison of subcellular pools of the metal without interfering signal from other compartments. Activation of the fluorescence in situ through a fluorogenic conjugation step effectively constrains the fluorescence signal to the locale of interest, thus improving the spatial resolution in imaging applications and eliminating the need for washout of mislocalized sensor. The labeling strategy is fully compatible with live cell imaging, and provides a valuable tool for tracking changes in metal distribution that to date have been an unsolved mystery in magnesium biology.

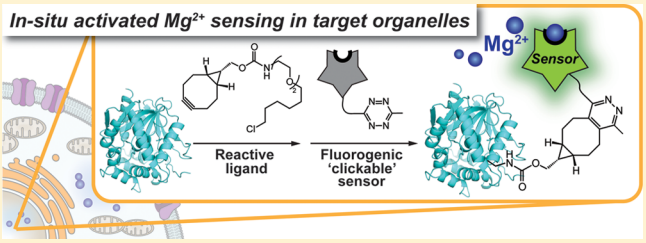

INTRODUCTION

Magnesium is an essential metal cation that is required as a cofactor for more than 600 enzymes, and plays important roles in regulation of ion transport, structural stabilization of nucleic acids and proteins, and as a second messenger.[1] Cellular levels of Mg^{2+} must be maintained within a narrow range optimal for cellular function.[1a] Regulation of cytosolic Mg^{2+} concentration involves a delicate balance between ion influx, efflux, buffering and compartmentalization within organelles. Despite much effort over the years, a litany of questions about the molecular players and the mechanisms involved in maintaining this balance still remain unanswered. A number of studies have demonstrated the ability of mammalian cells to undergo large changes in their total magnesium content upon metabolic or hormonal stimulation, without showing major changes in cytosolic concentrations of the free ion.[1a,2] These observations point to a redistribution of intracellular Mg^{2+} pools from various possible "intracellular stores"; the identity of these stores still remains under debate and a very limited toolbox is currently available to expose it.

The study of intracellular metal ion compartmentalization and trafficking involved in both physiologic and pathologic cellular processes demands sensors with controllable localization for the measurement of organelle-specific levels of the metal with subcellular resolution. This challenge has been partly met for some cations such as Ca^{2+} and Zn^{2+} with the advent of genetically encoded protein-based sensors. These sensors can be programmed, through the use of various localization sequences, to express in specific intracellular compartments thus enabling organelle-targeted detection.[3] The application of genetically encoded protein-based fluorescent sensors for the detection of other metals, however, has been limited. Merkx and co-workers recently reported the only example to date of a FRET protein-based sensor for Mg^{2+}, based on metal binding to a set of EF-hands from human centrin 3.[4] This sensor was targeted successfully to nuclei and to the cytosol but, unfortunately, showed limited response to conditions used to promote changes in intracellular Mg^{2+} levels in live cells. In comparison, the response of typical small-molecule metal indicators is faster and easier to tune than that of their protein-based counterparts. Their localization, however, is much more difficult to control, so their application in targeted detection of subcellular pools of metal ions is challenging. Oka and co-workers reported a small-molecule turn-on sensor for Mg^{2+} that shows spontaneous localization to mitochondria, presumably facilitated by a combination of positive charge and lipophilicity of the sensor.[5] Intensity-based sensors, however, provide a turn-on response that is dependent on sensor concentration and localization, thus prone to artifacts. In this regard, we recently reported a new *ratiometric* triazole-based Mg^{2+} indicator directed to mitochondria, which enabled metal quantification

Received: July 31, 2016
Published: October 17, 2016

DOI: 10.1021/jacs.6b07927
J. Am. Chem. Soc. 2016, 138, 14639−14649

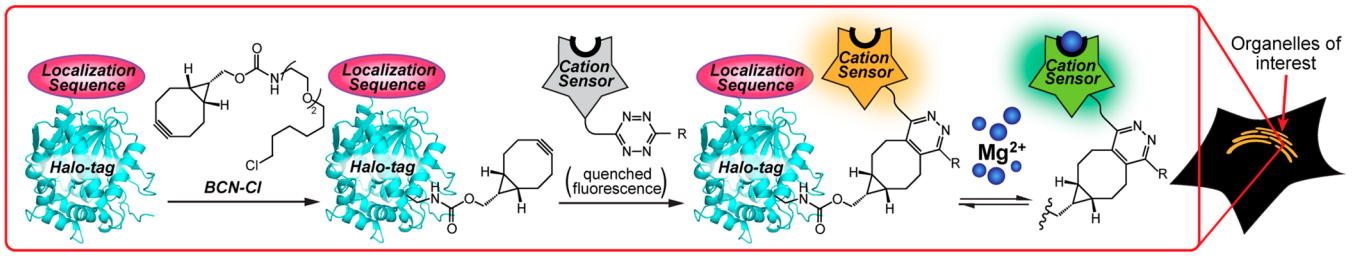

Figure 1. Two-step strategy for "on-demand" anchoring and activation of fluorescent metal indicator within intracellular organelles of interest, aimed at visualization of compartmentalized cations.

within the organelle and provided evidence of mitochondria-specific Mg^{2+} fluctuations taking place in early stages of cell death.[6]

The groups of Lippard and Johnsson described a hybrid sensing system that combines the ease of localization of genetically encoded O^6-alkyl guanine-DNA alkytransferase (AGT) fusion proteins with the advantageous sensing properties of a small molecule indicator for Zn^{2+}.[7] In their approach, a benzylguanine-functionalized derivative of the sensor acts as a substrate for the self-alkylating AGT domain and becomes covalently linked to the protein expressed in the desired cellular locale (SNAP-tag technology).[8] This strategy has been further applied in the context of Ca^{2+} sensing,[9] as well as in H_2O_2 detection.[10] A similar scheme has been employed for covalent attachment of fluorescent Zn^{2+}[11] and K^+[12] sensors to a membrane protein fused to a HaloTag, enabling detection of extracellular cations in the membrane vicinity. Oka and co-workers reported the fluorogenic intracellular attachment of a fluorescein-based biarsenical Mg^{2+} sensor to tetracysteine-tagged proteins in various intracellular compartments.[13] A critical step in the success of all previously reported hybrid strategies is the removal of unreacted small-molecule fluorophore to prevent spurious signal originating from undesired locales.[9a,12] For compounds with limited membrane permeability, however, complete washout is only possible after fixing the cells and permeabilizing the membrane, which precludes live cell applications. Significantly, many metal ion indicators for both main group and transition metals contain carboxylate-based metal-recognition groups that are most often loaded into cells as enzymatically cleavable ester derivatives;[14] once inside the cell, rapid hydrolysis of the esters and reveal of the carboxylates renders the compounds membrane impermeable and impossible to fully wash out without disrupting the cell membrane. With these severe constrains in mind, we sought to develop a system of general applicability for the targeted visualization of subcellular pools of metal ions with small-molecule fluorescent sensors. We introduce herein a novel two-step strategy designed to achieve both sensor anchoring and in situ activation of the fluorescence response within an organelle of choice, using a fluorogenic bioorthogonal reaction between a tetrazine-functionalized sensor and a strained alkyne conjugated to genetically encoded fusion proteins of known localization (Figure 1). We demonstrate that this new design is not limited by spontaneous localization of the sensor[15] and enables activation of the fluorescence "on demand", effectively constraining the signal to the subcellular locales of interest in a way that enables direct study of intracellular cation compartmentalization and trafficking, with improved resolution and low background.

RESULTS AND DISCUSSION

Design and Synthesis of a Tetrazine-Functionalized "Clickable" Ratiometric Sensor for on-Demand Activation. To enable "on-demand" cation detection within intracellular compartments, we devised a tetrazine-functionalized metal ion indicator whose fluorescence emission could be activated in the intracellular locale of choice by means of a biorthogonal reaction. A variety of tetrazines have been reported to quench the fluorescence of dyes with emission wavelengths between 400 and 600 nm through putative energy transfer mechanism; the quenching effect, however, is reduced or entirely abolished upon reaction of the tetrazine with strained alkenes.[16] This fluorogenic quality combined with favorable kinetics made the inverse electron demand Diels–Alder (iedDA) reaction between a tetrazine and strained alkene or alkyne partner an ideal choice for achieving both protein conjugation and activation of the fluorophore. With careful design of a suitable sensing moiety, a number of other fluorogenic systems developed for protein labeling purposes[17] could be adapted as well to obtain "on-demand" detection of various cellular targets.

To direct the sensor activation to specific organelles of interest and achieve signal compartmentalization, we envisioned a system that would exploit the HaloTag technology[18] as a means to install a reactive strained alkyne or alkene group on a protein of specific intracellular localization, through the recognition of a ligand containing such reactive moiety appended to a chloroalkane (e.g., BCN-Cl, Figure 1). This strategy circumvents the need for incorporation of a reactive group on the protein through encoding of unnatural amino acids,[19] and may enable fine-tuning by simple adjustments to the ligand. During the course of our studies, Fox and a group of researchers at Pfizer reported the covalent display of bioorthogonal groups on HaloTag fusion proteins through reaction with various chloroalkane ligands, designed for recognition by the dehalogenase domain.[20] These studies showed high efficiency in the fluorescent labeling of the fusion proteins providing further support for our design.

We chose to append a tetrazine moiety to Mag-*S*, a ratiometric Mg^{2+} sensor previously developed in our laboratory.[21] With an emission maximum at 547 nm in the Mg^{2+}-bound form, this sensor shows optimal spectral overlap with tetrazines for efficient quenching through a possible resonance energy transfer mechanism. The new tetrazine-functionalized sensor, **Mag-*S*-Tz** (Figure 2), was synthesized by a modification of the procedure employed for the synthesis of the parent Mag-*S* (Scheme 1). The fluorophore core was assembled by condensation of *tert*-butyl 2-(bromomethyl)-thiazole-5-carboxylate **1** with salicylaldehyde **2**,[22] which bears the ester-protected Mg^{2+}-recognition moiety. The *tert*-butyl

DOI: 10.1021/jacs.6b07927
J. Am. Chem. Soc. 2016, 138, 14639–14649

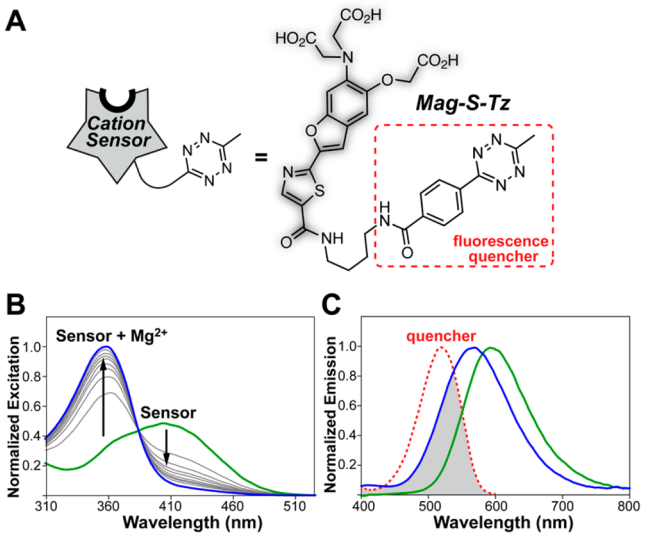

Figure 2. (A) Tetrazine-functionalized Mg^{2+} sensor, **Mag-*S*-Tz**, designed to be activated intracellularly through a fluorogenic reaction. Shaded portion of the structure corresponds to the parent Mag-*S* sensor. (B) Fluorescence excitation spectra of activated (treated with cyclooctyne BCN) **Mag-*S*-Tz** in response to increasing Mg^{2+} concentration; the large blue shift enables excitation ratiometric detection. (C) Normalized emission spectra of activated (treated with BCN) **Mag-*S*-Tz** in the Mg^{2+}-free and -bound forms (solid lines). The absorption spectrum of the tetrazine quencher (dashed line) overlaps well with the emission spectrum of the sensor, enabling efficient fluorescence quenching prior to reaction with an alkyne.

ester on the thiazole was then selectively hydrolyzed under acidic conditions to provide a unique attachment point for the tetrazine. Amide coupling with Boc-protected diamine **8** followed by ester hydrolysis and functionalization with tetrazine succinimide ester **9** yielded the weakly emissive **Mag-*S*-Tz**. A reference propylamide analogue **7**, devoid of the tetrazine moiety, was synthesized by a similar method.

Spectroscopic Properties of Activated Mag-*S*-Tz and HaloTag-Mag-*S*-Tz. The new amide bond on the 5-carboxy thiazole moiety of **Mag-*S*-Tz** leads to a shift of the absorption and emission spectra (λ_{abs} = 404 nm, λ_{em} = 595 nm, Table 1) to longer wavelengths compared to those of the parent acid, Mag-*S* (λ_{abs} = 396 nm, λ_{em} = 572 nm). This modest red shift may be rationalized as the effect of a greater stabilization of the intramolecular charge transfer (ICT) state provided by a neutral amide substituent in **Mag-*S*-Tz**, compared to a negatively charged carboxylate on the acceptor thiazole moiety in Mag-*S*. As anticipated, the attachment of the tetrazine decreases the quantum yield of the indicator significantly with respect to that of Mag-*S* both in the metal-free and -bound forms. The emission intensity increases up to 24-fold upon reaction with *endo*-9-hydroxymethyl-bicyclo[6.1.0]nonyne (BCN),[23] thus rendering the cycloaddition reaction fluorogenic (Table 1). Significantly, the quantum yield of the Diels–Alder product proved to be sensitive to the dienophile employed in the reaction, with the product of the cycloaddition of **Mag-*S*-Tz** with BCN being more emissive than the product of the reaction with the related *trans*-bicyclonene (sTCO,[24] data not shown). The dihydropyridazine products obtained from the reaction of tetrazines with strained *trans*-cyclooctenes have been reported to oxidize, sometimes in air, to yield pyridazines akin to those obtained from reaction with strained alkynes.[25,26] In the intracellular environment, however, the rate and extent of oxidation of the cycloaddition product may vary in an unpredictable manner, thus introducing unwanted variability in the fluorogenic efficiency of the reaction and complicating its applications in bioimaging. Accordingly, we chose to employ the strained alkyne BCN as the cycloaddition partner in order to attain a predictable product with known, stable emission properties, despite the compromise in reaction rate posed by this choice compared to a *trans*-cyclooctene.

Upon "switching on" the fluorescence via reaction with BCN, **Mag-*S*-Tz** responds to Mg^{2+} showing a 46 nm blue shift in its absorption spectrum (λ_{abs} = 358 nm, Table 1), which makes it suitable for excitation ratiometric detection of the cation with a dissociation constant K_d = 3.1 mM (Table 1 and Figures 2 and S1). The dissociation constant is appropriate for the detection of typical intracellular concentrations of Mg^{2+}, and is the same as that exhibited by the parent Mag-*S*.[21] These results show that attachment of the tetrazine moiety, or its cycloaddition products, does not affect the basic Mg^{2+}-binding properties of the sensor. Most significantly, the sensor undergoes the same blue shift in response to the cation when activated by a strained alkyne covalently attached to a protein domain (Figure S6). In its metal-bound form, however, the protein-conjugated sensor shows a roughly 2-fold lower quantum yield of fluorescence (Φ = 0.12) than the BCN-activated sensor, whereas in the metal-free state the protein-bound and BCN-activated species are equally emissive.

Overall, the activated **Mag-*S*-Tz** shows a similar metal selectivity profile to the parent Mag-*S* (Figure S2) and does not display significant changes in fluorescence ratio in the pH range spanning from 5.5 to 8.0 (Figure S3). Like most other sensors based on the *o*-aminophenol-*N*,*N*,*O*-triacetic acid (APTRA)

Scheme 1. Synthesis of Mag-S-Tz Sensor

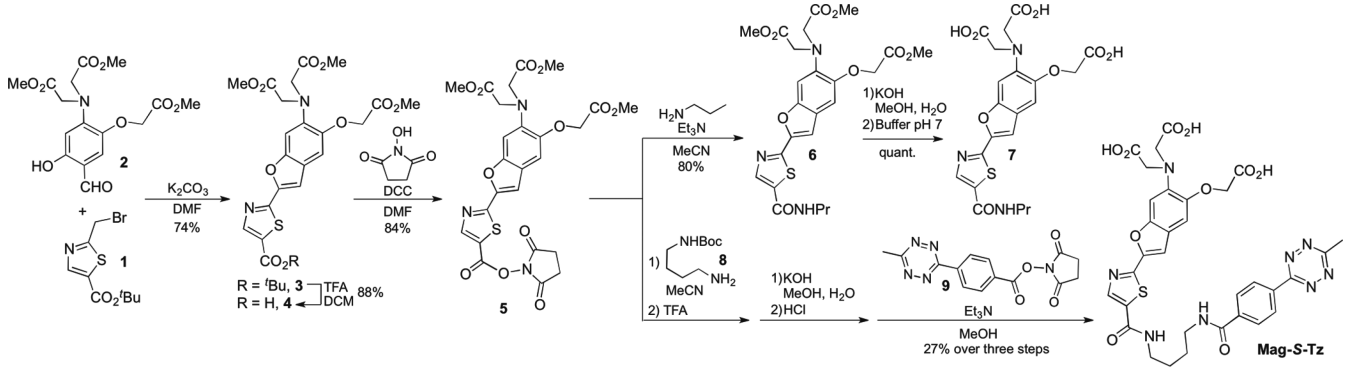

DOI: 10.1021/jacs.6b07927
J. Am. Chem. Soc. 2016, 138, 14639–14649

Table 1. Properties of New Mag-*S*-Tz Indicator and the Products of iedDA Reaction[a]

	absorption λ_{max} (nm), $\varepsilon \times 10^3$ (M^{-1} cm^{-1})		excitation λ_{max} (nm)		emission λ_{max} (nm), Φ[b]				
	unbound	Mg^{2+}-saturated	unbound	Mg^{2+}-saturated	unbound	Mg^{2+}-saturated	$K_{d,Mg^{2+}}$ (mM)	$K_{d,Ca^{2+}}$ (μM)	$K_{d,Zn^{2+}}$ (nM)
Mag-*S*[c]	396, 29.1	350, 30.1	392	347	572, 0.17	547, 0.30	3.2	38	62
Amide 7	404, 27.7(8)	358, 29(1)	404	358	595, 0.053(2)	565, 0.164(2)	N.D.	N.D.	N.D.
Mag-*S*-Tz	404	358	404	358	595, 0.0085(4)	565, 0.0101(5)	N.D.	N.D.	N.D.
Mag-*S*-Tz, activated	404	358	404	358	595, 0.100(4)	565, 0.24(1)	3.1(1)	40.6(8)	31(2)

[a]All properties measured in 50 mM PIPES, 100 mM KCl, pH 7.0, 25 °C. Molar absorptivity coefficients, fluorescence quantum yields and dissociation constants are averages of three independent determinations; numbers in parentheses represent the uncertainty on the last significant figure. N.D. = not determined. [b]Relative quantum yields were determined exciting at the excitation maximum of each fluorophore and using quinine sulfate in 0.5 M H_2SO_4 as standard (Φ = 0.546).[27] [c]Values from reference 21.

metal-binding group,[28] **Mag-*S*-Tz** also responds to high micromolar concentrations of Ca^{2+} or high nanomolar concentrations of Zn^{2+} (Table 1 and Figures S4 and S5). Such response makes this sensor a potential candidate for low-affinity detection of free Ca^{2+} or Zn^{2+} in biological samples with significantly elevated concentrations of these ions (vide infra).

The kinetics of the fluorogenic iedDA reaction between **Mag-*S*-Tz** and BCN were studied in aqueous buffer at pH 7 and 25 or 37 °C by monitoring the increase in fluorescence emission of the metal-free form of the indicator. The reactions were performed under pseudo-first-order conditions by incubating the tetrazine-functionalized sensor with fifty-fold higher concentration of BCN (Figure 3). Second order rate

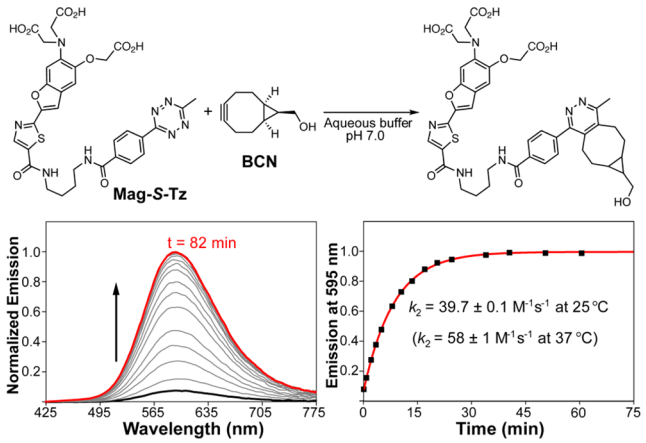

Figure 3. Kinetics of fluorogenic iedDA reaction of **Mag-*S*-Tz** with BCN in aqueous buffer at 25 °C. Shown in parentheses is the second order rate constant obtained from similar experiments conducted at 37 °C. Conditions: 1 μM of **Mag-*S*-Tz** and 50 μM BCN, λ_{exc} = 404 nm.

constants k_2 = 39.7 ± 0.1 M^{-1} s^{-1} at 25 °C and k_2 = 58 ± 1 M^{-1} s^{-1} at 37 °C were calculated from the increase in emission intensity. These values are consistent with previously reported rate constants for the reaction between BCN and 3,6-substituted tetrazines in methanol at room temperature, which have been shown to vary between 0.5 and 125 M^{-1} s^{-1} depending on the electronic properties of the tetrazine substituents.[29] In addition, we sought to study the kinetics of the iedDA reaction in a scenario that more closely resembled the desired intracellular fluorescence activation step, using a strained alkyne covalently attached to a HaloTag protein domain. For this purpose, purified recombinant His_6-HaloTag was incubated with three equivalents of BCN-Cl for 30 min at 37 °C, and then concentrated in a spin column to remove unreacted BCN-Cl. A solution of this alkyne-protein conjugate was treated with 7-fold lower concentration of **Mag-*S*-Tz** under similar conditions to those employed for the reaction with BCN. Analysis of the fluorescence emission over time afforded second order rate constants k_2 = 49 ± 4 M^{-1} s^{-1} at 25 °C and k_2 = 57 ± 3 M^{-1} s^{-1} at 37 °C, similar to those obtained for the reaction with the free alkyne (Figure S9 and S10). Attachment of BCN-Cl and **Mag-*S*-Tz** to the protein was confirmed by SDS-PAGE followed by in-gel fluorescence analysis (Figure S11), which shows a single, fluorescently labeled band for the adduct. These data indicate that protein conjugation does not have a significant effect on the reactivity of the strained alkyne toward iedDA. Furthermore, the rate constant for the reaction suggests that at concentrations typical of cell imaging experiments, sensor attachment and activation should be achieved within a few hours.

On-Demand Anchoring and Activation of Mag-*S*-Tz for Ratiometric Imaging of Mg^{2+} in Cellular Compartments. With a "clickable" Mg^{2+} indicator in hand, we focused on developing a protocol for on-demand activation of the fluorescence signal in intracellular organelles commonly invoked as possible regulators of magnesium compartmentalization.[1a,30] In our approach, control over the locale of fluorescence activation is provided by the choice of localization sequence fused to the HaloTag domain, which directs the expression of the protein to the organelle of interest. Fusion constructs pHTC-H2A, pHTC-Golgi and pCDNA3−4xMito-Halo targeting the nucleus, Golgi apparatus and mitochondria, respectively, were prepared. All the targeting vectors were built by appending HaloTag to the C-terminus of the respective targeting sequence. Construct pHTC-H2A contains the full length sequence of histone protein H2A,[31] whereas pHTC-Golgi uses the signaling sequence of β-1,4-galactosyltransferase that induces retention of the protein in the trans-Golgi.[32] The construct pCDNA3−4xMito-Halo includes four repeats of the localization sequence of cytochrome *c* oxidase subunit VIII, which directs the protein to the mitochondrial matrix.[3a] A nontargeted HaloTag, pHTN, was employed as well.

Intracellular activation of **Mag-*S*-Tz** was first tested in HEK 293T cells transiently expressing nontargeted HaloTag over the whole cell body. To facilitate cell uptake of the sensor, the negatively charged carboxylate groups were masked with acetoxymethyl (AM) esters that are readily cleaved by intracellular esterases.[33] For the intracellular formation of alkyne-protein conjugates, cells were incubated with 10 μM of BCN-Cl for 30 min at 37 °C followed by a 30 min incubation in fresh media to remove any unreacted alkyne. Next, cells were treated with 3 μM of membrane-permeable pro-sensor **Mag-*S***-

DOI: 10.1021/jacs.6b07927
J. Am. Chem. Soc. 2016, 138, 14639−14649

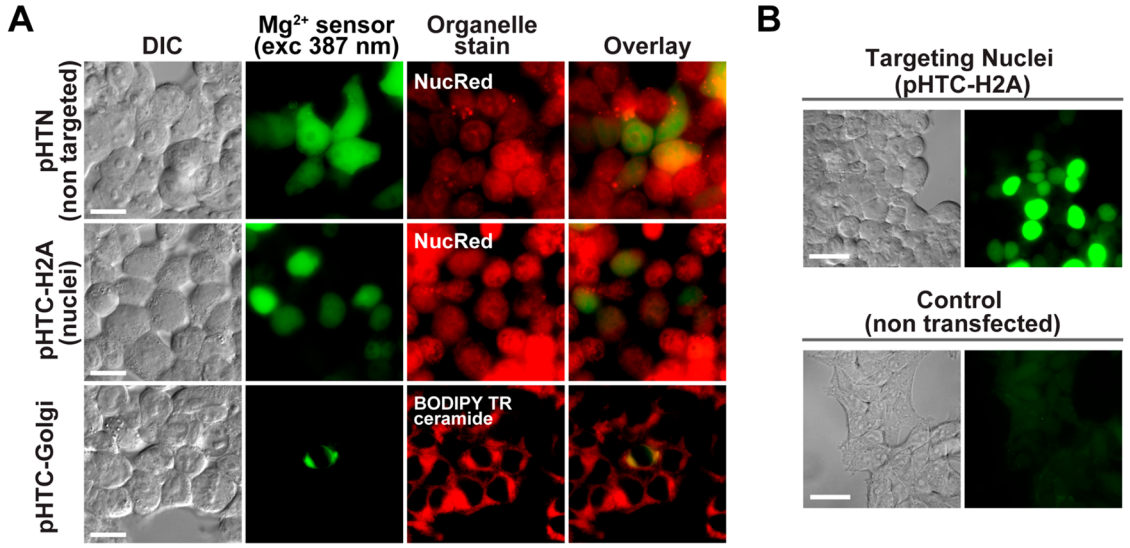

Figure 4. (A) Fluorescence microscopy images of live HEK 293T cells transiently expressing HaloTag fusion proteins in the whole cell body (top row), in the nucleus (middle) or in the Golgi (bottom), labeled via two-step strategy comprising treatment with BCN-Cl ligand followed by **Mag-*S*-Tz-AM** pro-sensor. Fluorogenic reaction between the protein-bound alkyne moiety and the tetrazine-functionalized cation sensor leads to fluorescence activation in the targeted compartment. Scale bar = 10 μm. (B) Comparison of microscopy images of cells expressing HaloTag-H2A in the nucleus (top) versus nontransfected controls (bottom) after treatment with BCN-Cl ligand followed by **Mag-*S*-Tz**. Scale bar = 20 μm.

Tz-AM and incubated for 60 min at 37 °C, followed by replacement of the growth medium and a 15 min incubation period at 37 °C to allow for complete de-esterification of the probe. Loading and de-esterification of **Mag-*S*-Tz-AM** were conducted in medium lacking FBS to prevent extracellular de-esterification of the sensor prior to cell uptake. Cells were then incubated in medium supplemented with 10% FBS at 37 °C for an additional 2−3 h to allow for the iedDA bioorthogonal reaction to occur. Successful intracellular fluorogenic activation of **Mag-*S*-Tz** was evidenced by bright fluorescence staining of the entire cell body of cells expressing the HaloTag protein (Figure 4A and S12). For comparison, control cells not expressing HaloTag showed negligible fluorescence above the background caused by autofluorescence, despite having been treated with the alkyne and fluorescent sensor under the same protocol (Figure 4B and S13). On average, transfected cells displayed a greater than 9-fold increase in fluorescence emission of the sensor for both the metal-bound and -free form in comparison to control, nontransfected cells. The staining pattern is fairly even, suggesting that the small molecules BCN and **Mag-*S*-Tz** do not show a preferential localization pattern of their own.

In situ conjugation and activation of **Mag-*S*-Tz** within intracellular compartments of interest was then pursued, using the general staining protocol outlined above (Figure 4A). Successful labeling of the Golgi apparatus in HEK 293T cells transiently expressing pHTC-Golgi was evidenced by a Pearson correlation coefficient of 0.83 in a colocalization analysis with Golgi stain BODIPY TR Ceramide (Molecular Probes), as shown in Figure S14. This analysis was conducted over the three-dimensional volume of the cell reconstructed from a series of z-stacked images. Organelle-specific activation of the fluorescence response was also achieved in the nucleus, as demonstrated by the staining pattern observed in cells expressing pHTC-H2A (Figure 4A). Because of the spectral overlap with **Mag-*S*-Tz**, standard Hoechst 33342 nuclear stain could not be employed as the reference stain for colocalization analysis. An alternative red nuclear stain, namely Nuc Red Live 647 (Molecular Probes), was employed instead, but spurious signal originating from poor localization of this dye hampered quantitative colocalization analysis. In the case of cells transfected with pCDNA3−4xMito-Halo, unfortunately, the protein expression levels were very low, leading to weak fluorescence signal with the labeling protocol employed for other compartments (data not shown). Further optimization of the transfection system will be necessary to ensure sufficient protein expression and sensor activation for imaging purposes.

Comparison of the signal originating in nuclei of cells transiently expressing the Histone-HaloTag protein with that from cells in a control plate, or from neighboring cells within the same plate but not expressing the protein, shows the marked increase in fluorescence elicited by the intracellular iedDA reaction (Figure 4B and S13). The low fluorescence background from other, nontargeted compartments demonstrates that unreacted BCN-Cl was washed out effectively in all cases, and that fluorescence activation due to nonspecific interactions of either BCN-Cl or **Mag-*S*-Tz** with biomolecules is not a problem. Significantly, the good signal-to-noise ratio achieved in the fluorescence activation step eliminates the requirement for washout of the membrane-impermeable **Mag-*S*-Tz**, which would require some form of membrane permeabilization; the ease of removal of the small, membrane permeable BCN-Cl is key to maintaining the integrity of the cell membrane and to the success of the overall strategy. Viability assays conducted after the various steps show no significant decrease in cell viability caused by our sensor loading and activation protocol (Figure S20). As such, our strategy is fully compatible with live cell imaging and tracking, in real time, of changes in metal ion distribution.

The intracellularly activated, protein-conjugated **Mag-*S*-Tz** effectively responds to Mg^{2+}, affording ratiometric detection of organelle-specific chelatable pools of this ion. Treatment of cells with 30 mM $MgCl_2$ and nonfluorescent ionophore 4-bromo A-23187 for 20 min leads to an increase in the average fluorescence ratio in either targeted organelles or over the whole cell body (Figure 5), demonstrating the ability of the

DOI: 10.1021/jacs.6b07927
J. Am. Chem. Soc. 2016, 138, 14639−14649

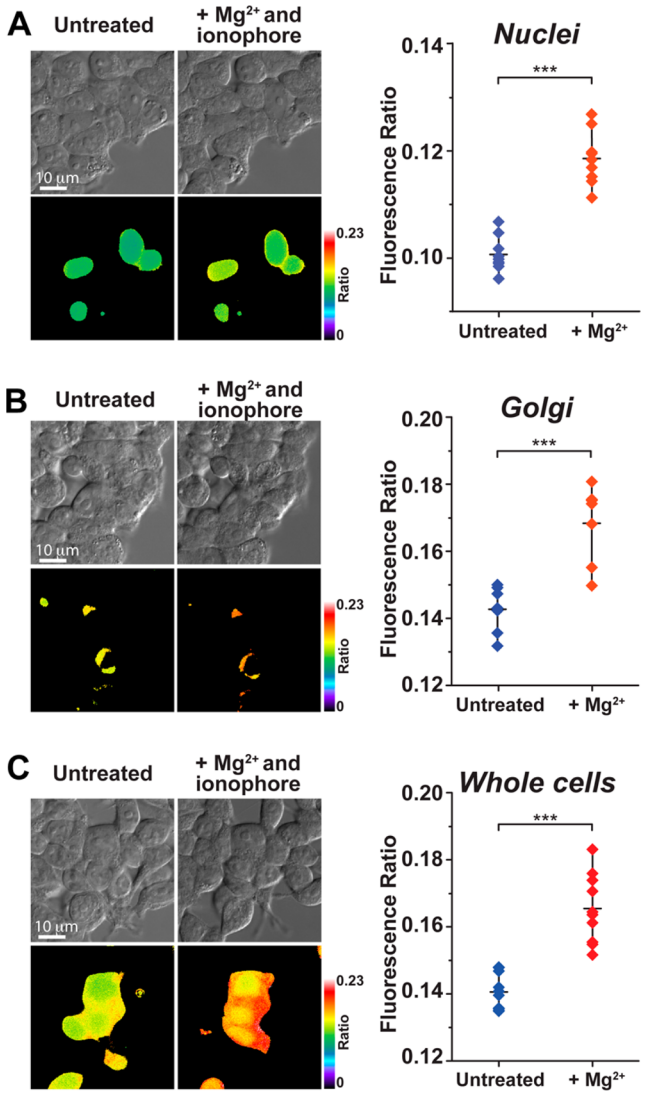

Figure 5. Ratiometric microscopy imaging of Mg^{2+} with sensor **Mag-*S*-Tz** activated on demand in nuclei (A), Golgi (B), or in the whole cell (C). Left: fluorescence ratio images before and after treatment with 30 mM Mg^{2+} and ionophore 4-Br-A-23187. Right: plots showing the change in fluorescence ratio reflecting the rise in intracellular Mg^{2+} concentration mediated by the ionophore. Fluorescence ratio in untreated cells corresponds to detection of basal (endogenous) levels of Mg^{2+} in the respective compartment. Ratio = Intensity at 340 nm excitation/Intensity at 387 nm excitation. ***$P \leq 0.001$; *t*-test.

sensor to report on fluctuations in the Mg^{2+} concentration in various compartments.[34] Notably, in the absence of added exogenous Mg^{2+}, the basal fluorescence ratio obtained in the nucleus is significantly lower than the ratio obtained in the Golgi or cytosol under the same imaging conditions, which indicates that the concentration of the endogenous chelatable Mg^{2+} is lower in the former. In this regard, the nucleus has been considered an important cellular store for Mg^{2+}, which plays important roles in maintaining genomic stability.[30] To date, however, limited information is available regarding physiological levels of this cation in nuclei of mammalian cells. Staining patterns of nontargeted fluorescent sensors in various cell lines have suggested both higher and lower levels of chelatable Mg^{2+} in this organelle with respect to other compartments.[35] These patterns, however, are likely dependent on the cell type and may have been influenced by the spatial distribution of the fluorescent sensor as much as that of the metal, particularly in studies conducted with intensity-based turn-on sensors.

As suggested by the characterization of **Mag-*S*-Tz** in vitro, the sensor could respond to high concentrations of Zn^{2+} or Ca^{2+}. To rule out the possible interference of either of these cations in the detection of Mg^{2+}, especially in the Ca^{2+}-rich Golgi apparatus,[36] a series of imaging experiments was conducted in the presence of selective chelators used for their sequestration. Specifically, treatment of cells with 10 to 25 μM of BAPTA-AM, an intracellular Ca^{2+} chelator, did not cause a significant change in the fluorescence ratio of the indicator, demonstrating that basal Ca^{2+} levels do not interfere with the detection of endogenous Mg^{2+} (Figure S15). Furthermore, the treatment with BAPTA did not affect the change in fluorescence ratio induced by treatment with exogenous $MgCl_2$ + ionophore, confirming that the sensor is responding to changes in intracellular Mg^{2+} and not to possible mobilization of Ca^{2+} by the ionophore. Similarly, treatment of **Mag-*S*-Tz** labeled cells with 10 μM of Zn^{2+} chelator TPEN did not induce significant changes in the measured fluorescence ratio in the various compartments, ruling out the detection of endogenous free Zn^{2+} by the sensor (Figure S16). Moreover, addition of TPEN did not alter the response of sensor to treatment with exogenous Mg^{2+} and ionophore (Figure S17), thus corroborating that the observed fluorescence changes are induced by changes in intracellular Mg^{2+} content and not by adventitious mobilization of Zn^{2+} by the ionophore. It is important to emphasize that the natural compartmentalization of metal cations in the cell, which leads to accumulation of high levels of certain metals in some organelles, imposes more stringent demands on the selectivity profile of sensors used for targeted detection and must be considered in the overall design of the imaging experiments and controls. Our results demonstrate that the use of selective chelators may be employed to rule out potential artifacts caused by minor cross-reactivity of the sensor. The study of Mg^{2+} compartmentalization can, therefore, be accomplished with the sensing system described herein in cell lines that are not especially rich in Ca^{2+} or Zn^{2+}.

Although the experiments described above provided no evidence of **Mag-*S*-Tz** response to endogenous levels of Ca^{2+} or Zn^{2+} in HEK 293T cells, we sought to test whether the sensor could be exploited as low-affinity indicator for these divalent cations in biological systems that are particularly metal rich. For this purpose, a rapid rise in metal concentration was induced via treatment with exogenous Ca^{2+} or Zn^{2+} internalized with ionophores ionomycin or pyrithione, respectively. Cells expressing nontargeted HaloTag were stained with **Mag-*S*-Tz** as per the protocol outlined above and incubated with ionomycin and 10 mM $CaCl_2$, which led to an ~62% increase in the fluorescence ratio throughout the whole cell within ~10 min (Figure S18). A large fluorescence ratio increase was also observed upon treatment with 50 μM of $ZnCl_2$ in a one-to-one stoichiometry mixture with pyrithione, demonstrating the ability of the protein-anchored indicator to report on the changes in metal levels present in its microenvironment (Figure S19). It is conceivable that, with a choice of sensor with the appropriate metal recognition unit, the strategy introduced herein could be easily extended to study physiological levels of other metal ions or analytes, enabling the study of cellular compartmentalization and redistribution involved in the regulation of metal homeostasis or in signaling.

DOI: 10.1021/jacs.6b07927
J. Am. Chem. Soc. 2016, 138, 14639−14649

CONCLUSIONS

Intracellular distribution of metal cations is anything but homogeneous. The development of fluorescent sensors for the targeted detection of cations in specific organelles has been instrumental in shedding light on metal compartmentalization and translocation, and their role in signaling and cellular homeostasis. Whereas important advances have been made in the subcellular detection of Ca^{2+} and Zn^{2+}, primarily owed to the development of genetically encoded, protein-based sensors incorporating cellular localization sequences, progress in the targeted detection of other cations has been slow. Hybrid platforms that combine the easily tunable, fast response of small-molecule fluorescent sensors with the genetically encodable localization properties of proteins represent a valuable option, particularly for metals for which conserved binding sequences with the right affinity and selectivity have not been identified or successfully implemented into all-protein sensors. We introduced herein a new strategy for activation of fluorescent sensing "on demand" within intracellular organelles of choice, using a fast fluorogenic reaction between a tetrazine-functionalized small-molecule pro-sensor, **Mag-*S*-Tz**, and a strained bicyclononyne covalently linked to a genetically encoded HaloTag fusion protein of known cellular localization. Through a simple two-step protocol, protein conjugation was achieved within a couple of hours and was shown to preserve the metal-binding properties of the APTRA-based fluorescent indicator. The sensor displayed a dissociation constant K_d = 3.1 mM suitable for the detection of low millimolar concentrations of chelatable Mg^{2+} typical of the intracellular environment.

The fluorogenic nature of the conjugation reaction provides unique advantages to our strategy that are worth highlighting. Specifically, it provides a chemical means to constrain the fluorescence signal to the subcellular locale where the fusion protein is expressed, thus limiting the interference from unreacted indicator present in neighboring compartments and improving the spatial resolution. Furthermore, activation of the fluorescence in situ eliminates the need for washout of unreacted membrane-impermeable indicator via disruption of the cell membrane. Our strategy is, therefore, fully compatible with live cell imaging and enables the real time visualization of changes in metal ion distribution involved in cellular processes.

We demonstrated the application of our sensing system in the ratiometric detection of Mg^{2+} in target organelles such as the nucleus and Golgi apparatus of HEK 293T cells, providing the first direct comparison of subcellular chelatable pools of the metal without interfering signal from other compartments that revealed lower concentration of free Mg^{2+} in the cell nucleus. Because efficient quenching by tetrazines has been shown for a variety of fluorophores with emission in the visible range, we anticipate that the strategy presented herein might be readily extended to a wide range of sensors, many of which are carboxylate-rich and could not be applied in similar strategies before. As such, we expect this strategy to become a valuable tool for addressing current questions in the cell biology of metals and of other important targets.

EXPERIMENTAL SECTION

General Synthetic Protocols. Salicylaldehyde 2,[37] *tert*-butyl (4-aminobutyl)carbamate 8,[38] tetrazine NHS ester 9,[39] and *endo*-BCN[23] were prepared according to literature procedures. The syntheses of BCN-Cl and of *tert*-butyl 2-(bromomethyl)thiazole-5-carboxylate (1) from ethyl 2-methylthiazole-5-carboxylate[40] are detailed in the Supporting Information. All other reagents were purchased from commercial sources and used as received. Solvents were purified and degassed by standard procedures. NMR spectra were acquired on Bruker Avance 400 spectrometers or Bruker Avance 600 spectrometer equipped with a triple resonance CPTCI cryoprobehead. ^{1}H NMR chemical shifts are reported in ppm relative to $SiMe_4$ (δ = 0) and were referenced internally with respect to residual protio impurity in the solvent (δ = 7.26 for $CHCl_3$, 2.50 for DMSO-d_5, 5.32 for $CHDCl_2$, 3.31 for CHD_2OD, 1.94 for CHD_2CN). ^{13}C NMR chemical shifts are reported in ppm relative to $SiMe_4$ (δ = 0) and were referenced internally with respect to the solvent signal (δ 77.16 for $CDCl_3$, 39.52 for DMSO-d_6, 53.84 for CD_2Cl_2, 49.00 for CD_3OD, 1.32 for CD_3CN). Coupling constants are reported in Hz. Melting points were collected on a BUCHI 510 melting point apparatus and are reported uncorrected. Low-resolution mass spectra were acquired on an Agilent 1100 series LC/MSD trap spectrometer, using electrospray (ES) ionization. High-resolution mass spectrometry (HRMS) analyses were conducted on an Agilent 6224 TOF LC/MS Mass Spectrometer using ES ionization. Analytical thin layer chromatography (TLC) was performed on SorbTech polyester backed 200 μm silica gel sheets. Reversed-phase HPLC analyses were conducted on an Agilent 1260 system with UV−vis absorption and fluorescence detection, using a Poroshell C18 reversed phase column (4.6 × 50 mm, 2.7 μm particle size) and eluting with a gradient of 10% to 100% acetonitrile/water (+ 0.1% trifluoroacetic acid) over 7 min.

Synthesis of 2(5(*tert*-Butoxycarbonyl)thiazol-2-yl)-6-amino-5-hydroxy-benzofuran-*N*,*N*,*O*-triacetic Acid Trimethyl Ester, 3. A solution of salicylaldehyde 2 (100 mg, 0.27 mmol), *tert*-butyl 2-(bromomethyl)thiazole-5-carboxylate 1 (113 mg, 0.41 mmol), and K_2CO_3 (187 mg, 1.35 mmol) in dry dimethylformamide (2.0 mL) was heated to 100 °C under inert atmosphere for 1.5 h. After allowing to cool to room temperature, the reaction was poured into water (30 mL) and extracted with EtOAc (3 × 30 mL). The combined extracts were dried over Na_2SO_4 and concentrated in vacuo. The residue was purified by column chromatography on silica gel (1:1 EtOAc/hexanes) to give product 3 as a yellow solid (110 mg, 74%, R_f = 0.38 in 1:1 hexanes/EtOAc). mp 129−130 °C. ^{1}H NMR (400 MHz, $CDCl_3$, δ) 8.32 (s, 1H), 7.31 (s, 1H), 7.10 (s, 1H), 7.04 (s, 1H), 4.70 (s, 2H), 4.27 (s, 4H), 3.80 (s, 3H), 3.75 (s, 6H), 1.60 (s, 9H). ^{13}C{^{1}H} NMR (100 MHz, $CDCl_3$, δ) 171.5, 169.4, 162.3, 160.7, 151.9, 149.5, 149.1, 148.2, 140.5, 130.7, 122.4, 107.1, 107.0, 102.9, 83.0, 67.1, 54.0, 52.3, 52.1, 28.4. ESI-MS (m/z): $[M + H]^+$ calcd for $C_{25}H_{28}N_2O_{10}S$, 549.2; found 549.2.

Synthesis of 2(5-Carboxythiazol-2-yl)-6-amino-5-hydroxy-benzofuran-*N*,*N*,*O*-triacetic Acid Trimethyl Ester, 4. A solution of compound 3 (38 mg, 0.069 mmol) in dichloromethane (0.8 mL) was treated with trifluoroacetic acid (0.2 mL) and stirred at room temperature overnight. The volatiles were evaporated and the residue was recrystallized in ethyl acetate/hexanes to give compound 4 as a yellow solid (30 mg, 88%, R_f = 0.37 in 10:1 CH_2Cl_2/MeOH). mp 145−146 °C (decomp.). ^{1}H NMR (400 MHz, DMSO-d_6, δ) 8.34 (s, 1H), 7.52 (s, 1H), 7.20 (s, 1H), 7.14 (s, 1H), 4.82 (s, 2H), 4.26 (s, 4H), 3.71 (s, 3H), 3.64 (s, 6H). ^{13}C{^{1}H} NMR (100 MHz, DMSO-d_6, δ) 170.9, 169.1, 162.1, 160.6, 150.8, 148.5, 148.4, 147.2, 139.9, 131.8, 120.8, 107.2, 105.9, 101.5, 65.7, 53.4, 51.9, 51.5. ESI-MS (m/z): $[M + H]^+$ calcd for $C_{21}H_{20}N_2O_{10}S$, 493.1; found 493.1.

Synthesis of 2(5(Succinimidylcarboxy)thiazol-2-yl)-6-amino-5-hydroxy-benzofuran-*N*,*N*,*O*-triacetic Acid Trimethyl Ester, 5. A solution of compound 4 (30 mg, 0.061 mmol) and *N*-hydroxysuccinimide (8 mg, 0.067 mmol) in dry dimethylformamide (1 mL) was stirred at room temperature for 5 min. Then a solution of DCC (15 mg, 0.073 mmol) in dry dimethylformamide (0.3 mL) was added. The reaction mixture was stirred at room temperature overnight. The white precipitate was filtered off and the filtrate was concentrated in vacuo. The residue was purified by column chromatography on silica gel (1:1 EtOAc/hexanes) to give product 5 as a yellow solid (30 mg, 84%, R_f = 0.58 in EtOAc). mp 164−165 °C. ^{1}H NMR (600 MHz, DMSO-d_6, δ) 8.89 (s, 1H), 7.73 (d, J = 0.7 Hz, 1H), 7.24 (s, 1H), 7.14 (s, 1H), 4.84 (s, 2H), 4.28 (s, 4H), 3.72 (s, 3H), 3.64 (s, 6H), 2.90 (s, 4H). ^{13}C{^{1}H} NMR (150 MHz, DMSO-d_6, δ) 170.9, 170.2, 169.1, 164.2, 156.7, 153.4, 151.5, 147.5, 147.3, 140.8,

DOI: 10.1021/jacs.6b07927
J. Am. Chem. Soc. 2016, 138, 14639−14649

120.6, 109.7, 105.8, 101.2, 65.6, 53.5, 51.9, 51.6, 25.6. ESI-MS (m/z): $[M + H]^+$ calcd for $C_{25}H_{23}N_3O_{12}S$, 590.1; found 590.5.

Synthesis of 2(5(Propylaminocarbonyl)thiazol-2-yl)-6-amino-5-hydroxy-benzofuran-*N,N,O*-triacetic Acid Trimethyl Ester, 6. To a solution of compound 5 (7.0 mg, 12 μmol) and propylamine (1.5 μL, 18 μmol) in MeCN (1.0 mL) was added Et_3N (20 μL) and the reaction mixture was stirred at room temperature for 1 h. The solvent was evaporated and the residue was redissolved in EtOAc (5.0 mL). The resulting solution was washed with water (3 × 10 mL), dried over Na_2SO_4 and concentrated in vacuo. The residue was purified by column chromatography on silica gel (40:1 CH_2Cl_2/MeOH) to give compound 6 as a yellow solid (5.2 mg, 80%, R_f = 0.56 in 19:1 CH_2Cl_2/MeOH). mp 169−170 °C. ^{1}H NMR (400 MHz, CD_3CN, δ): 8.20 (s, 1H), 7.34 (d, J = 0.8 Hz, 1H), 7.15 (t, J = 5.3 Hz, 1H), 7.11 (d, J = 0.8 Hz, 1H), 7.10 (s, 1H), 4.73 (s, 2H), 4.23 (s, 4H), 3.75 (s, 3H), 3.67 (s, 6H), 3.32−3.27 (m, 2H), 1.65−1.55 (m, 2H), 0.95 (t, J = 7.4 Hz, 3H). $^{13}C\{^1H\}$ NMR (100 MHz, CD_3CN, δ):172.2, 170.3, 161.2, 161.0, 152.2, 150.4, 148.8, 144.8, 141.1, 136.1, 122.7, 107.2, 107.0, 103.1, 67.0, 54.5, 52.7, 52.3, 42.3, 23.4, 11.7. HR-TOF-MS (m/z): $[M + H]^+$ calcd for $C_{24}H_{27}N_3O_9S$, 534.15408; found 534.15647.

Preparation of Compound 7 (Quantitative Stock Solution for Fluorescence Spectroscopy). A sample of ester 6 (2.13 mg, 0.0040 mmol) in methanol (40 μL) was treated with aqueous potassium hydroxide (40 μL, 1.2 M, 0.048 mmol) and stirred at room temperature for 24 h. The solution was quantitatively transferred to a volumetric flask and diluted with buffer at pH 7.0 (50 mM PIPES, 100 mM KCl) to a final volume of 2 mL. Quantitative hydrolysis was verified by HPLC. The stock solution was divided into small aliquots, flash frozen in liquid nitrogen, and stored below −20 °C.

Synthesis of Mag-*S*-Tz. A mixture of succinimidyl ester 5 (30 mg, 0.051 mmol) and *tert*-butyl (4-aminobutyl)carbamate 8 (15 mg, 0.076 mmol) in acetonitrile (1.5 mL) was treated with two drops of triethylamine and stirred at room temperature for 30 min. The white precipitate was filtered off and the filtrate was concentrated in vacuo and redissolved in dichloromethane (0.8 mL). The resulting solution was treated with trifluoroacetic acid (0.2 mL) and stirred at room temperature for 1 h. The volatiles were evaporated and the residue was redissolved in dichloromethane (20 mL). The solution was washed with aqueous K_2CO_3 (20 mL, 1 M), dried over Na_2SO_4 and concentrated in vacuo. To the residue was added methanol (600 μL) and aqueous KOH (300 μL, 1.2 M), and the mixture was stirred at room temperature overnight. The reaction solution was neutralized with aqueous HCl and lyophilized. The residue was dissolved in MeOH (3 mL) and triethylamine (10 μL) and tetrazine 9 (20 mg, 0.064 mmol) were added. The reaction mixture was stirred at room temperature for 30 min and concentrated in vacuo. The residue was purified by reversed phase semipreparative HPLC to give Mag-*S*-Tz as a red solid (10 mg, 27%). mp 230−231 °C. ^{1}H NMR (400 MHz, DMSO-d_6, δ) 12.5 (br, 3H), 8.76 (t, J = 5.6 Hz, 1H), 8.72 (t, J = 5.6 Hz, 1H), 8.54 (d, J = 8.6 Hz, 2H), 8.45 (s, 1H), 8.10 (d, J = 8.6 Hz, 2H), 7.49 (d, J = 0.6 Hz, 1H), 7.16 (s, 1H), 7.07 (s, 1H), 4.72 (s, 2H), 4.19 (s, 4H), 3.33 (overlapping solvent), 3.01 (s, 3H), 1.62 (s, 4H). $^{13}C\{^1H\}$ NMR (100 MHz, DMSO-d_6, δ) 172.1, 170.2, 167.3, 165.4, 162.9, 159.6, 159.5, 150.7, 148.3, 147.5, 144.1, 140.0, 137.9, 135.2, 134.1, 128.2, 127.3, 120.6, 106.8, 105.5, 101.4, 65.6, 53.5, 39.1, 26.6, 20.9. ESI-MS (m/z): $[M + H]^+$ calcd for $C_{32}H_{30}N_8O_{10}S$, 719.2; found 719.1.

Synthesis of Mag-*S*-Tz Acetoxymethyl Ester, Mag-*S*-Tz-AM. A mixture of compound Mag-*S*-Tz (0.21 mg, 0.3 μmol) in dimethylformamide (300 μL) was treated with diisopropylethylamine (10 μL, 100 μmol) and bromomethyl acetate (5 μL, 50 μmol) at room temperature for 1 h, protected from light. The mixture was purified by reversed phase semipreparative HPLC to give Mag-S-Tz-AM as a red solid (0.11 mg, 40%). HR-TOF-MS (m/z): $[M + H]^+$ calcd for $C_{41}H_{42}N_8O_{16}S$, 935.25112; found 935.25166.

General Spectroscopic Methods. All aqueous solutions were prepared using deionized water having a resistivity of 18 MΩ/cm. Other solvents were obtained from commercial vendors and used as received. Piperazine-*N,N*-bis(2-ethanesulfonic acid) (PIPES), 99.999% KCl, 99.999% $MgCl_2$, 99.999% $ZnCl_2$, 99.99% $CaCl_2$, and high-purity 25% HCl, 45% KOH, and 50% NaOH were purchased from Sigma-Aldrich. Stock solutions of the sensors in their acid form were stored at −20 °C in 100−200 μL aliquots, and thawed immediately before each experiment. Spectroscopic measurements at pH 7.0 were conducted in aqueous buffer containing 50 mM PIPES and 100 mM KCl. Measurements containing purified HaloTag protein were conducted at in 50 mM PIPES buffer at pH 7. Buffers were treated with Chelex resin (Bio-Rad) to remove adventitious metal ions according to the manufacturer's protocol, unless otherwise noted. Measurements of pH were conducted using a Mettler Toledo FE20 with glass electrode. UV−visible spectra were acquired on a Cary 100 spectrophotometer using 1 cm quartz cuvettes. Fluorescence spectra were acquired on a QuantaMaster 40 Photon Technology International spectrofluorometer equipped with xenon lamp source, emission and excitation monochromators, excitation correction unit, and PMT detector. Emission spectra were corrected for the detector wavelength-dependent response. The excitation spectra were corrected for the wavelength-dependent lamp intensity. Measurements were conducted at 25.0 ± 0.1 °C or 37.0 ± 0.1 °C. Extinction coefficients were determined in the 0−11 μM range in aqueous buffer at pH 7.0, in the absence or presence of 200 mM Mg^{2+} for the metal-free and -bound forms of the sensor, respectively. Fluorescence quantum yields were determined using 0.5−3.0 μM solutions of the sensor in aqueous buffer at pH 7.0, exciting at the reported excitation maxima for each compound. Solutions of quinine in 0.5 M aqueous sulfuric acid, with a reported quantum yield of 0.546 upon excitation at 347 nm, were used as standards.[27] Fluorescence emission spectra were integrated from 360 to 680 nm.

Activation of Mag-*S*-Tz for Fluorescence Spectroscopy by Reaction with *endo*-BCN. A solution of Mag-*S*-Tz in DMSO (2 mM, 50 μL) was mixed with a solution of *endo*-BCN in DMSO (20 mM, 50 μL) and incubated at room temperature for 1 h, protected from light. The resulting solution was divided into small aliquots, flash frozen in liquid nitrogen, and stored below −20 °C. Aliquots of this stock solution were thawed immediately prior to use and diluted in aqueous buffer to the desired concentration for photophysical studies.

Metal Selectivity Profile. Metal selectivity measurements were performed using 0.5 μM BCN-activated sensor in aqueous buffer at pH 7.0. Emission spectra with excitation at 358 nm and at 404 nm were recorded before and after treatment with either $CaCl_2$, $MnCl_2$, $Fe(NH_4)_2(SO_4)_2$, $CoCl_2$, $NiCl_2$, $CuCl_2$, or $ZnCl_2$ in aqueous buffer, for a final concentration of 5 μM M^{n+} or 5 μM M^{n+} and 200 mM $MgCl_2$. Integrated fluorescence emission was employed for the calculation of the fluorescence ratio.

Study of pH-Dependent Response. Emission spectra (λ_{exc1} = 358 nm, λ_{exc2} = 404 nm) of a 0.5 μM solution of BCN-activated sensor were acquired in aqueous buffers at pH ranging from 5.5 to 8.0. Aqueous MES buffers (100 mM KCl, 50 mM MES) were used in the pH range from 5.5 to 6.5. Aqueous HEPES buffers (100 mM KCl, 50 mM HEPES) were used in the pH range from 7.0 to 8.0. For measurements of the ratio in the metal-free form, 5 μM of EDTA was applied to chelate residual metals. For the metal-saturated experiment, measurements were conducted in the presence of 200 mM $MgCl_2$. Integrated fluorescence emission was employed for the calculation of the fluorescence ratio.

Determination of Metal Dissociation Constants. Fluorescence titrations with Mg^{2+} and Ca^{2+} were conducted using 1 μM solutions of the BCN-activated Mag-*S*-Tz sensor in aqueous buffer at pH 7.0, covering a range of 0−500 mM for $[Mg^{2+}]_t$ and 0−2 mM for $[Ca^{2+}]_t$. Excess metal was employed to confirm the saturation value. Magnesium was added from a 1000 mM $MgCl_2$ stock solution. Calcium was added from a 10 mM $CaCl_2$ stock solution. For each titration, the metal stock solution was treated with an appropriate amount of the sensor to match the concentration in the cuvette and prevent sensor dilution throughout the experiment. Fluorescence titrations with Zn^{2+} were conducted using 0.5 μM solutions of the sensor in aqueous buffer at pH 7.0. Metal concentration was adjusted using a Zn^{2+}/EGTA buffered system, with 1 mM EGTA and total

DOI: 10.1021/jacs.6b07927
J. Am. Chem. Soc. 2016, 138, 14639−14649

concentration of Zn^{2+} (from $ZnCl_2$) ranging from 0 to 1 mM. Details of data fitting are provided in the Supporting Information.

Kinetic Studies of Fluorescence Activation of Mag-*S*-Tz with BCN. The activation of Mag-*S*-Tz with *endo*-BCN was studied under pseudo-first-order conditions at 25 °C and at 37 °C. The two reactants were dissolved separately in DMSO, and then mixed together in 3 mL of aqueous buffer pH 7.0 for a final concentration of 1 μM Mag-*S*-Tz and 50 μM *endo*-BCN at 25 °C, or 0.5 μM Mag-*S*-Tz and 25 μM BCN at 37 °C. Emission spectra (λ_{exc} = 404 nm) were collected periodically over 3 h. For each experiment, the pseudo-first-order rate constant, k_{obs}, was obtained from exponential fit of the fluorescence intensity at 595 nm as a function of time, as described in detail in the Supporting Information. The second order rate constant, k_2, was calculated from the pseudo-first-order rate constant.

Kinetic Studies of the Fluorescence Activation of Mag-*S*-Tz with Protein-Anchored BCN (HaloTag-BCN). Hexahistidine-tagged HaloTag (pH6HTN His_6HaloTag, Promega) was overexpressed in BL21 *E. coli* cells and purified with a standard Ni-NTA affinity column. Purified HaloTag in 0.5 mL of PBS (final concentration 10 μM) was treated with BCN-Cl (for a final concentration of 30 μM) for 30 min at 37 °C. The mixture was concentrated followed by four buffer exchanges with 50 mM PIPES buffer using an Amicon Ultra-0.5 Centrifugal Filter Unit with Ultracel-10 membrane (Millipore) to remove unreacted BCN-Cl. Protein concentration in the final solution was determined with a Bradford assay. The reaction between Mag-*S*-Tz and HaloTag-BCN was studied under pseudo-first-order conditions. The two reactants were mixed in a micro cuvette with a final volume of 250 μL, for a final concentration of 1 μM Mag-*S*-Tz and ∼7 μM HaloTag-BCN. The reaction was maintained at 25 or 37 °C, and emission spectra (λ_{exc}= 404 nm) were acquired periodically over 5.5 h. The k_{obs} were obtained from analysis of fluorescence intensity at 595 nm as a function of time, as detailed in the Supporting Information. Second order rate constants k_2 were calculated from the pseudo-first-order rate constants. Binding of the BCN-Cl and Mag-*S*-Tz to HaloTag was confirmed by SDS-PAGE followed by in gel-fluorescence exciting with UV light and Coomassie blue protein staining. Images were acquired on Syngene Gbox iChemi XT.

Spectroscopic Properties of HaloTag-Mag-*S*-Tz in Response to Mg^{2+}, Ca^{2+}, and Zn^{2+}. Purified HaloTag was treated with BCN-Cl in 0.5 mL of PBS (for a final concentration of 15 μM protein and 45 μM BCN-Cl) and incubated at 37 °C for 30 min. The reaction was concentrated and subjected to four buffer exchanges with PIPES buffer using an Amicon Ultra-0.5 Centrifugal Filter Unit with Ultracel-10 membrane (Millipore) to remove excess BCN-Cl. The functionalized protein was brought to a concentration of 50 μM, treated with 5 μM of Mag-*S*-Tz, and allowed to react for 5.5 h protected from light. The solution was diluted for a final concentration of 0.5 μM in clicked sensor. Excitation scans were acquired before and after treatment with $MgCl_2$, $CaCl_2$ or $ZnCl_2$ solution for a final concentration of 200 mM Mg^{2+}, 2 mM Ca^{2+}, or 2 μM of Zn^{2+}.

Cell Culture and Imaging Protocols. HEK 293T cells were cultured in Dulbecco's Modified Eagle Medium (DMEM) supplemented with 10% fetal bovine serum (FBS), 50 U/mL Penicillin, and 50 μg/mL Streptomycin at 37 °C in a 5% CO_2 humidified atmosphere. Cells were seeded in 35 mm glass bottom cell culture dishes (MatTek) and after 24 h were transfected with the appropriate construct (see Supporting Information for details on targeting vectors) using Lipofectamine 3000 (Life Technologies) according to manufacturer protocols. Cells were imaged 24−48 h after transfection. Fluorescence imaging experiments were performed on a Leica DMI6000B inverted fluorescence microscope equipped with a Hamamatsu ORCA-Flash 4.0 CCD camera, scanning stage, high-speed filter wheel for excitation filters and a mercury metal halide external light source. For ratiometric imaging of Mag-*S*-Tz, a Leica Fura-2 excitation filter set was paired with a YFP emission filter. A Leica Texas Red filter cube was employed for imaging of BODIPY TR Ceramide (Molecular Probes) and a Chroma Cy5 Narrow Excitation filter cube was used for imaging of NucRed Live 647 Ready Probe (Molecular Probes). Crosstalk experiments were conducted with the various filter/dye combinations, ruling out bleed-through of the organelle tracker dye signal into the sensor channels and vice versa. The microscope was operated with Leica LAS AF software. Image processing for ratio determination was performed with Metamorph 7.7.0.0 software. For fluorescence ratio images, background correction and thresholds were applied to individual images prior to ratio calculation. Deconvolution of z-stacked images was performed with Autoquant X3.0.2 using iterative restoration algorithms; colocalization analyses were performed over the reconstructed cell volumes.

General Protocol for Indicator Loading and In Situ Fluorescence Activation. Cells grown in complete growth media (transfected with the appropriate vector 24 to 48 h prior to imaging) were incubated with 10 μM BCN-Cl for 30 min at 37 °C, in a 5% CO_2 humidified atmosphere. The cells were washed two times with growth media, bathed in 2 mL of fresh media and incubated for another 30 min at 37 °C to enable washout of unbound chloroalkane ligand. Cells were then washed two times with FBS-free DMEM and incubated for 1 h at 37 °C in FBS-free DMEM (2 mL) containing 3 μM Mag-*S*-TZ-AM added from a stock solution of the sensor suspended in 20% Pluronic F-127 according to manufacturers protocol (final concentration of Pluronic in the plate is 0.015%). After this period, the medium was replaced with fresh FBS-free DMEM (2 mL) and cells were allowed to stand for an additional 15 min at 37 °C to ensure complete de-esterification of the sensor. After de-esterification, the medium was replaced with complete growth medium and the cells were incubated at 37 °C for 2 to 3 h to allow additional time for the iedDA reaction to occur. Organelle stains BODIPY TR Ceramide (5 μM, Molecular Probes) or NucRed Live 647 Ready Probe (Molecular Probes) were added during the final 30 min of incubation at 37 °C. Prior to imaging, the cells were washed with the imaging medium (2 mL) and bathed in the imaging medium (1 mL) for image acquisition. For localization studies, cells were imaged in Live Cell Imaging Solution (Life Technologies). For studies involving metal ion manipulation, cells were imaged in HHBSS with no divalent cations.

Imaging of Mg^{2+} in HEK 293T Cells. Cells were cultured and stained as described in the general protocol, and were bathed in HHBSS with no divalent cations (1 mL) during image acquisition. To confirm the sensor's response to Mg^{2+}, cells were treated on the microscope stage with medium supplemented with additional $MgCl_2$ and nonfluorescent ionophore 4-bromo A-23187 (Molecular Probes) for a total concentration of 30 mM cation and 30 μM ionophore in the plate. For comparison, images before and after 20 min treatment with excess Mg^{2+} and ionophore were acquired and processed under identical conditions, and are shown on the same ratio scale. Control experiments to rule out detection of endogenous Zn^{2+} or Ca^{2+}, or adventitious mobilization of these cations by the ionophore, were conducted as follows: cells stained as previously described were treated with 10 μM TPEN on the microscope stage and imaged over a period of 20 min. In a separate experiment, stained cells were treated with 30 mM $MgCl_2$ and 30 μM 4-bromo A-23187 for 20 min followed by the addition of 10 μM TPEN and imaged over a period of 20 min. To rule out Ca^{2+} interference in the detection, cells stained with Mag-*S*-Tz as described above were treated with 10 to 25 μM BAPTA-AM (Molecular Probes) for 30 min at 37 °C in DMEM lacking FBS. Cells were washed with HHBSS with no divalent cations and incubated for another 20 min at room temperature to enable deesterification of the chelator. Images were acquired before and after treatment with 30 mM $MgCl_2$ and 30 μM 4-bromo A-23187. For comparison, images before and after treatment were acquired and processed under identical conditions.

Low-Affinity Imaging of Ca^{2+} or Zn^{2+} in HEK 293T Cells. To test the response of the sensor to high concentrations of Ca^{2+} or Zn^{2+}, cells cultured and stained as described in the general protocol were treated on the microscope stage with medium supplemented with $CaCl_2$ and ionomycin (Molecular Probes) for a total concentration of 10 mM and 10 μM, respectively; or with Zn^{2+}-pyrithione in a 1:1 ratio, for a total concentration of 50 μM each. Images before and after treatment with excess metal and ionophore were acquired and processed under identical conditions, and are shown on the same ratio scale.

DOI: 10.1021/jacs.6b07927
J. Am. Chem. Soc. 2016, 138, 14639−14649

Cell Viability Studies. CellTiter-Glo Luminescent Cell Viability Assay (Promega) was performed to assess the toxicity of the cell labeling protocol with Mag-*S*-Tz and the treatment with exogenous Mg^{2+}. HEK 293T cells were plated in a white opaque 96 well plate and transfected with pHTC-H2A the following day. Twenty-four h post transfection, cells were treated with BCN-Cl and Mag-*S*-Tz-AM as described in the general cell loading procedure above. Cells were then incubated with 30 mM $MgCl_2$ and 30 μM 4-bromo A-23187 for 30 min. CellTiter-Glo was added to the wells as described by the manufacturer's protocol. Control experiment was performed in the same fashion, using DMSO as vehicle. The luminescence was read on using a SynergyHT Microplate Reader.

■ ASSOCIATED CONTENT

Supporting Information

The Supporting Information is available free of charge on the ACS Publications website at DOI: 10.1021/jacs.6b07927.

Additional figures, synthesis of precursors, details of data fitting protocols, and spectroscopic characterization data for all new compounds (PDF)

■ AUTHOR INFORMATION

Corresponding Author

*dbuccella@nyu.edu

Author Contributions

†J.J.G. and G.Z. contributed equally.

Notes

The authors declare no competing financial interest.

■ ACKNOWLEDGMENTS

This work was supported by the National Science Foundation under award CHE-1555116, and by start-up funds from New York University to D.B. The Bruker Avance 400 NMR spectrometer was acquired with support of National Science Foundation under award number CHE-01162222. The CPTCI-cryoprobehead was acquired through the support of the National Institutes of Health S10 grant under award number OD016343.

■ REFERENCES

(1) (a) Romani, A. M. P. *Arch. Biochem. Biophys.* **2011**, *512*, 1. (b) Li, F.-Y.; Chaigne-Delalande, B.; Kanellopoulou, C.; Davis, J. C.; Matthews, H. F.; Douek, D. C.; Cohen, J. I.; Uzel, G.; Su, H. C.; Lenardo, M. J. *Nature* **2011**, *475*, 471. (c) de Baaij, J. H. F.; Hoenderop, J. G. J.; Bindels, R. J. M. *Physiol. Rev.* **2015**, *95*, 1.

(2) (a) Fatholahi, M.; LaNoue, K.; Romani, A.; Scarpa, A. *Arch. Biochem. Biophys.* **2000**, *374*, 395. (b) Murphy, E. *Circ. Res.* **2000**, *86*, 245. (c) Romani, A. *Arch. Biochem. Biophys.* **2007**, *458*, 90.

(3) (a) Rizzuto, R.; Simpson, A. W. M.; Brini, M.; Pozzan, T. *Nature* **1992**, *358*, 325. (b) Palmer, A. E.; Tsien, R. Y. *Nat. Protoc.* **2006**, *1*, 1057. (c) Dittmer, P. J.; Miranda, J. G.; Gorski, J. A.; Palmer, A. E. *J. Biol. Chem.* **2009**, *284*, 16289. (d) Vinkenborg, J. L.; Koay, M. S.; Merkx, M. *Curr. Opin. Chem. Biol.* **2010**, *14*, 231.

(4) Lindenburg, L. H.; Vinkenborg, J. L.; Oortwijn, J.; Aper, S. J. A.; Merkx, M. *PLoS One* **2013**, *8*, e82009.

(5) Shindo, Y.; Fujii, T.; Komatsu, H.; Citterio, D.; Hotta, K.; Suzuki, K.; Oka, K. *PLoS One* **2011**, *6*, e23684.

(6) Zhang, G.; Gruskos, J. J.; Afzal, M. S.; Buccella, D. *Chem. Sci.* **2015**, *6*, 6841.

(7) Tomat, E.; Nolan, E. M.; Jaworski, J.; Lippard, S. J. *J. Am. Chem. Soc.* **2008**, *130*, 15776.

(8) Keppler, A.; Gendreizig, S.; Gronemeyer, T.; Pick, H.; Vogel, H.; Johnsson, K. *Nat. Biotechnol.* **2003**, *21*, 86.

(9) (a) Bannwarth, M.; Correa, I. R.; Sztretye, M.; Pouvreau, S.; Fellay, C.; Aebischer, A.; Royer, L.; Rios, E.; Johnsson, K. *ACS Chem. Biol.* **2009**, *4*, 179. (b) Kamiya, M.; Johnsson, K. *Anal. Chem.* **2010**, *82*, 6472.

(10) (a) Srikun, D.; Albers, A. E.; Nam, C. I.; Iavarone, A. T.; Chang, C. J. *J. Am. Chem. Soc.* **2010**, *132*, 4455. (b) Abo, M.; Minakami, R.; Miyano, K.; Kamiya, M.; Nagano, T.; Urano, Y.; Sumimoto, H. *Anal. Chem.* **2014**, *86*, 5983.

(11) Li, D.; Liu, L.; Li, W.-H. *ACS Chem. Biol.* **2015**, *10*, 1054.

(12) Hirata, T.; Terai, T.; Yamamura, H.; Shimonishi, M.; Komatsu, T.; Hanaoka, K.; Ueno, T.; Imaizumi, Y.; Nagano, T.; Urano, Y. *Anal. Chem.* **2016**, *88*, 2693.

(13) Fujii, T.; Shindo, Y.; Hotta, K.; Citterio, D.; Nishiyama, S.; Suzuki, K.; Oka, K. *J. Am. Chem. Soc.* **2014**, *136*, 2374.

(14) (a) Domaille, D. W.; Que, E. L.; Chang, C. J. *Nat. Chem. Biol.* **2008**, *4*, 168. (b) Dean, K. M.; Qin, Y.; Palmer, A. E. *Biochim. Biophys. Acta, Mol. Cell Res.* **2012**, *1823*, 1406. (c) Trapani, V.; Schweigel-Roentgen, M.; Cittadini, A.; Wolf, F. I. *Methods Enzymol.* **2012**, *505*, 421. (d) Carter, K. P.; Young, A. M.; Palmer, A. E. *Chem. Rev.* **2014**, *114*, 4564. (e) Yin, J.; Hu, Y.; Yoon, J. *Chem. Soc. Rev.* **2015**, *44*, 4619.

(15) Indicators loaded into cells as Acetoxymethyl (AM) esters tend to show spontaneous compartmentalization that is difficult to control, and often requires special loading conditions. See: Haugland, R. P. *Handbook of Fluorescent Probes and Research Products*, 9th ed.; Molecular Probes Inc.: Eugene, OR, 2002.

(16) Devaraj, N. K.; Hilderbrand, S.; Upadhyay, R.; Mazitschek, R.; Weissleder, R. *Angew. Chem., Int. Ed.* **2010**, *49*, 2869.

(17) (a) Komatsu, T.; Johnsson, K.; Okuno, H.; Bito, H.; Inoue, T.; Nagano, T.; Urano, Y. *J. Am. Chem. Soc.* **2011**, *133*, 6745. (b) Hori, Y.; Nakaki, K.; Sato, M.; Mizukami, S.; Kikuchi, K. *Angew. Chem., Int. Ed.* **2012**, *51*, 5611. (c) Shieh, P.; Dien, V. T.; Beahm, B. J.; Castellano, J. M.; Wyss-Coray, T.; Bertozzi, C. R. *J. Am. Chem. Soc.* **2015**, *137*, 7145. (d) Walker, A. S.; Rablen, P. R.; Schepartz, A. *J. Am. Chem. Soc.* **2016**, *138*, 7143.

(18) Los, G. V.; Encell, L. P.; McDougall, M. G.; Hartzell, D. D.; Karassina, N.; Zimprich, C.; Wood, M. G.; Learish, R.; Ohana, R. F.; Urh, M.; Simpson, D.; Mendez, J.; Zimmerman, K.; Otto, P.; Vidugiris, G.; Zhu, J.; Darzins, A.; Klaubert, D. H.; Bulleit, R. F.; Wood, K. V. *ACS Chem. Biol.* **2008**, *3*, 373.

(19) Lang, K.; Davis, L.; Wallace, S.; Mahesh, M.; Cox, D. J.; Blackman, M. L.; Fox, J. M.; Chin, J. W. *J. Am. Chem. Soc.* **2012**, *134*, 10317.

(20) Murrey, H. E.; Judkins, J. C.; am Ende, C. W.; Ballard, T. E.; Fang, Y.; Riccardi, K.; Di, L.; Guilmette, E. R.; Schwartz, J. W.; Fox, J. M.; Johnson, D. S. *J. Am. Chem. Soc.* **2015**, *137*, 11461.

(21) Afzal, M. S.; Pitteloud, J.-P.; Buccella, D. *Chem. Commun.* **2014**, *50*, 11358.

(22) Levy, L. A.; Murphy, E.; Raju, B.; London, R. E. *Biochemistry* **1988**, *27*, 4041.

(23) Dommerholt, J.; Schmidt, S.; Temming, R.; Hendriks, L. J. A.; Rutjes, F. P. J. T.; van Hest, J. C. M.; Lefeber, D. J.; Friedl, P.; van Delft, F. L. *Angew. Chem., Int. Ed.* **2010**, *49*, 9422.

(24) Taylor, M. T.; Blackman, M. L.; Dmitrenko, O.; Fox, J. M. *J. Am. Chem. Soc.* **2011**, *133*, 9646.

(25) (a) Knall, A.-C.; Slugovc, C. *Chem. Soc. Rev.* **2013**, *42*, 5131. (b) Wu, H.; Yang, J.; Šečkutė, J.; Devaraj, N. K. *Angew. Chem., Int. Ed.* **2014**, *53*, 5805.

(26) In our own studies, the dihydropyridazine products obtained from reaction with TCO appeared to oxidize upon exposure to air over the course of several hours. The oxidation led to changes in the fluorescence efficiency of the compound.

(27) Brouwer, A. M. *Pure Appl. Chem.* **2011**, *83*, 2213.

(28) Brady, M.; Piombo, S. D.; Hu, C.; Buccella, D. *Dalton Trans.* **2016**, *45*, 12458.

(29) (a) Chen, W.; Wang, D.; Dai, C.; Hamelberg, D.; Wang, B. *Chem. Commun.* **2012**, *48*, 1736. (b) Wang, D.; Chen, W.; Zheng, Y.; Dai, C.; Wang, K.; Ke, B.; Wang, B. *Org. Biomol. Chem.* **2014**, *12*, 3950.

(30) Hartwig, A. *Mutat. Res., Fundam. Mol. Mech. Mutagen.* **2001**, *475*, 113.

(31) Goedhart, J.; von Stetten, D.; Noirclerc-Savoye, M.; Lelimousin, M.; Joosen, L.; Hink, M. A.; van Weeren, L.; Gadella, T. W. J.; Royant, A. *Nat. Commun.* **2012**, *3*, 751.
(32) (a) Llopis, J.; McCaffery, J. M.; Miyawaki, A.; Farquhar, M. G.; Tsien, R. Y. *Proc. Natl. Acad. Sci. U. S. A.* **1998**, *95*, 6803. (b) Russo, R. N.; Shaper, N. L.; Taatjes, D. J.; Shaper, J. H. *J. Biol. Chem.* **1992**, *267*, 9241.
(33) Tsien, R. Y. *Nature* **1981**, *290*, 527.
(34) The changes in ratio indicate that the sensor is present in the de-esterified, metal-responsive form in all compartments tested. Although it is not clear that this form can move between organelles after de-esterification, the presence of esterases in almost every subcellular compartment ensures that the permeable, acetoxymethyl ester-protected form can be activated in the various organelles it reaches. See: (a) Satoh, T.; Hosokawa, M. *Annu. Rev. Pharmacol. Toxicol.* **1998**, *38*, 257. (b) Mentlein, R.; Rix-Matzen, H.; Heymann, E. *Biochim. Biophys. Acta, Gen. Subj.* **1988**, *964*, 319.
(35) (a) Quamme, G. A.; Dai, L. J.; Rabkin, S. W. *Am. J. Physiol. Heart Circ. Physiol.* **1993**, *265*, H281. (b) Gotoh, H.; Kajikawa, M.; Kato, H.; Suto, K. *Brain Res.* **1999**, *828*, 163. (c) Komatsu, H.; Iwasawa, N.; Citterio, D.; Suzuki, Y.; Kubota, T.; Tokuno, K.; Kitamura, Y.; Oka, K.; Suzuki, K. *J. Am. Chem. Soc.* **2004**, *126*, 16353. (d) Farruggia, G.; Iotti, S.; Prodi, L.; Montalti, M.; Zaccheroni, N.; Savage, P. B.; Trapani, V.; Sale, P.; Wolf, F. I. *J. Am. Chem. Soc.* **2006**, *128*, 344.
(36) Pinton, P.; Pozzan, T.; Rizzuto, R. *EMBO J.* **1998**, *17*, 5298.
(37) Raju, B.; Murphy, E.; Levy, L. A.; Hall, R. D.; London, R. E. *Am. J. Physiol. Cell Physiol.* **1989**, *256*, C540.
(38) Singh, P.; Samori, C.; Toma, F. M.; Bussy, C.; Nunes, A.; Al-Jamal, K. T.; Menard-Moyon, C.; Prato, M.; Kostarelos, K.; Bianco, A. *J. Mater. Chem.* **2011**, *21*, 4850.
(39) Yu, C.; Qian, L.; Uttamchandani, M.; Li, L.; Yao, S. Q. *Angew. Chem.* **2015**, *127*, 10720.
(40) Mashraqui, S. H.; Keehn, P. M. *J. Am. Chem. Soc.* **1982**, *104*, 4461.

DOI: 10.1021/jacs.6b07927
J. Am. Chem. Soc. 2016, 138, 14639−14649